Nano Res. 2012, 5(12): 863–874
DOI 10.1007/s12274-012-0270-x
Research Article

ISSN 1998-0124
CN 11-5974/O4

Drastically Increased Absorption in Vertical Semiconductor Nanowire Arrays: A Non-Absorbing Dielectric Shell Makes the Difference

Nicklas Anttu[1,§] (✉), Kousar L. Namazi[1,§], Phillip M. Wu[1,§] (✉), Pengfei Yang[2], Hongxing Xu[1,2], H. Q. Xu[1,3], and Ulf Håkanson[1,2]

[1] Division of Solid State Physics/The Nanometer Structure Consortium at Lund University (nmC@LU), P.O. Box 118, S-221 00 Lund, Sweden
[2] Beijing National Laboratory for Condensed Matter Physics, Institute of Physics, Chinese Academy of Sciences, P.O. Box 603-146, Beijing 100190, China
[3] Department of Electronics and Key Laboratory for the Physics and Chemistry of Nanodevices, Peking University, Beijing 100871, China
[§] N. A., K. N., and P. M. W. contributed equally to this work and are co-first authors

Received: 16 August 2012 / Revised: 10 October 2012 / Accepted: 11 October 2012

ABSTRACT

Enhanced absorption of especially long wavelength light is needed to enable the full potential of semiconductor nanowire (NW) arrays for optoelectronic applications. We show both experimentally and theoretically that a transparent dielectric shell (Al_2O_3 coating) can drastically improve the absorption of light in InAs NW arrays. With an appropriate thickness of the Al_2O_3 shell, we achieve four times stronger absorption in the NWs compared to uncoated NWs and twice as good absorption as when the dielectric completely fills the space between the NWs. We provide detailed theoretical analysis from a combination of full electrodynamic modeling and intuitive electrostatic approximations. This reveals how the incident light penetrates better into the absorbing NW core with increasing thickness of the dielectric shell until a resonant shell thickness is reached. We provide a simple description of how to reach this strongly absorbing resonance condition, making our results easy to apply for a broad wavelength range and a multifold of semiconductor and dielectric coating material combinations.

KEYWORDS

Nanowire array, InAs, absorption, photovoltaics, core–shell, Al_2O_3 coating

1. Introduction

Vertical arrays [1, 2] of Ⅲ–Ⅴ semiconductor nanowires (NWs) are currently attracting intense research interest for optoelectronic devices like solar cells [3–9], photodetectors [10], lasers [11], and light-emitting diodes [12]. Much of this interest stems from the advantages in the material synthesis of NWs compared to bulk layers. Strain relaxation in the radial direction in the NW geometry [13] allows for a wide range of materials to be combined epitaxially in the axial [14, 15] or radial direction [16], also on cheap substrates [12], in combinations not accessible in bulk layer growth due to too large crystal lattice mismatch. This allows for novel material architectures for enhanced functionality in optoelectronics.

Address correspondence to Nicklas Anttu, nicklas.anttu@ftf.lth.se; Phillip M. Wu, phillipmwu@gmail.com

For photovoltaics and photodetection, two of the major advantages of using NW arrays are the possibility of (i) tailoring [7] the materials composition, and therefore the band gaps, in the active region much more freely than in bulk devices and (ii) growing NWs of technologically important but abundant/expensive materials on cheap substrates [7, 12]. In core–shell NWs where a pn-junction is defined in the radial direction, the NW geometry allows furthermore for efficient absorption along the NW axis whereas efficient charge-separation occurs in the radial direction [7]. In axially defined NW heterostructures the materials (and therefore the band gaps) of a multi-junction solar cell can be chosen to effectively match [17] the solar spectrum, giving the prospect of cheap next-generation high-efficiency photovoltaics with NW arrays [7]. However, efficient absorption of long wavelength photons in NW arrays is problematic [18] and needs to be enhanced for more optimum performance.

Here, we show experimentally and theoretically how common dielectric coating techniques [5, 7, 19–21] in nanoscience can be used for achieving strongly enhanced absorption in the NWs for a broad wavelength range. With an appropriate thickness of the dielectric shell surrounding the absorbing NW core, more than four times as strong light absorption in the NWs can be achieved compared to completely bare (uncoated) NWs and more than twice as strong compared to the case in which the dielectric completely fills out the space between the NWs. In short, the shell thickness makes the difference—"*just enough*" boosts the light capture of the NWs considerably, whereas neither "*less is more*" nor "*more is more*" are the optimal design strategies.

In more detail, we have quantitatively investigated with light scattering spectroscopy the reflection properties of an InAs NW array when consecutively depositing thin layers of Al_2O_3 as dielectric coating (Fig. 1(a)). At first glance, we find a reduced reflectance with increasing coating thickness, as expected from thin-film models based on (partially) destructive interference in the reflected light [22]. We find, however, also spectral shifts in the reflectance not expected from such simple models, indicating that more sophisticated analysis is needed.

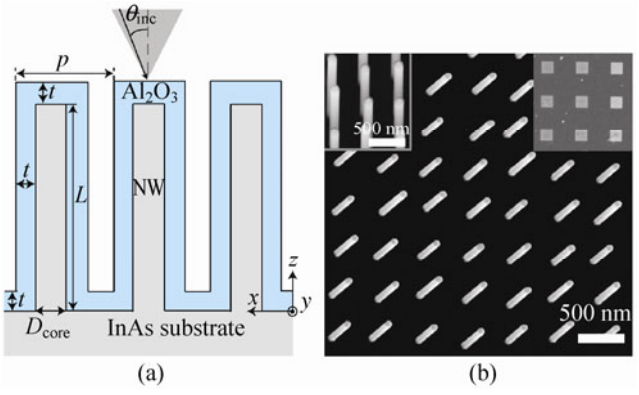

Figure 1 (a) Schematic view of an InAs NW array coated with Al_2O_3 of thickness t. The NWs are of diameter D_{core} and length L and stand in a square array of period p on top of an InAs substrate. The shaded triangle indicates the cone from which unpolarized light is incident from and collected into by an objective lens with NA = 0.5 (half angle of 30°). We depict here also the polar angle θ_{inc}. The azimuth angle φ_{inc} (not shown) is zero when the incidence plane is parallel to the x and z axis and 90° when it is parallel to the y and z axis. (b) SEM image (at a tilt of 10° from top view) showing 7 × 7 NWs of the array with p = 450 nm, D_{core} = 62 nm, and L = 2040 nm that this work concentrates on. Left inset: SEM image (at 20° tilt) after deposition of 30 nm Al_2O_3 onto the NWs in (b). Right inset: Top view SEM image of the nine fabricated NW arrays, each of 50 μm × 50 μm in size

We present theoretical results from full electrodynamical modeling and find very good quantitative agreement with the experimental reflectance measurements. This modeling moreover allows for the study of the absorption of light in the NWs, which is not readily measurable in the experiments. We find that the absorptance of the NWs increases considerably when the NWs are coated. To provide an intuitive explanation of the underlying physical mechanism of this absorption enhancement, we describe first the interaction of light with the NWs in the electrostatic limit. We find that the shell allows for enhanced penetration of the electric field of the incident light into the core of the NWs, leading to stronger absorption. Full electrodynamic modeling, beyond the electrostatic limit, shows that strong electric field concentration into the core of the NWs is possible for a wide range of coating thicknesses. This occurs when the fundamental waveguide mode of the core–shell NW system is strongly excited and leads to an enhancement of the absorption by more than a factor of four compared to uncoated NWs.

2. Experimental

As a model system, we choose to work with an array of InAs NWs coated with Al_2O_3. InAs has a low room temperature band gap of $E_g = 0.34$ eV giving rise to a strong bulk absorption in the visible wavelength range that we study. This allows for easily detectable optical response even from dilute arrays of NWs of modest lengths [18]. The procedures and main results of this work are, however, of general character and not limited to the exact choice of the semiconductor material of the NWs or the dielectric coating used here.

For the experimental investigations, nine periodic arrays of InAs NWs were grown in a high vacuum chemical beam epitaxy (CBE) unit (see Methods for details). Each array, of area 50 μm × 50 μm and square lattice, was defined by gold (Au) dots defined by electron beam lithography (EBL). Al_2O_3 was deposited at 250 °C, as depicted in Fig. 1(a), onto the NWs by means of atomic layer deposition (ALD) [19, 21] (Cambridge Nanotech Savannah system) in consecutive cycles/steps. The optical reflectance of the array was measured after each deposition cycle/step. In this way, we explore experimentally the effect on the optical response of a given initial InAs NW array when increasing the Al_2O_3 coating thickness in a controlled manner. Each of the first four cycles/steps consisted of deposition of 10 nm oxide on the NWs, resulting in a 20 nm increase in the (total) diameter of the NWs after each cycle [23][1]. A final oxide deposition cycle of 30 nm was done to investigate the optical response of a core–shell system with a fairly thick shell layer of approximately the same thickness as the core diameter. A scanning electron microscope (SEM) was used to accurately determine the NW core diameter D_{core}, NW length L, array period p, as well as the thickness t of the deposited Al_2O_3 layer. Since the NW arrays covered only a small area of the substrate surface, we could also measure the reflectance of the bare InAs substrate after each ALD step.

The broadband light reflection measurements were performed in the wavelength range of 400 nm < λ < 850 nm with a Zeiss optical microscope equipped with an optical probe (Filmetrics F40). In the measurements, unpolarized light was incident from a 20x objective (Numerical Aperture (NA) = 0.5), generating an illumination cone of 30° half angle (Fig. 1(a)), oriented normal to the array. The reflected light, from a square spot of an area of 20 μm × 20 μm, was collected with the same objective and sent to a spectrometer. Background and baseline calibrations were performed using a silicon reference substrate.

The nine fabricated arrays of InAs NWs (see inset in Fig. 1(b)) had different periods p ranging from 450 to 650 nm and lengths L from 1500 nm to 3800 nm. All these arrays showed in the reflectance spectra similar shape before deposition of any Al_2O_3 and similar changes when depositing the Al_2O_3 layers. For brevity, we concentrate here on one representative array of period $p = 450$ nm and NWs of length $L = 2040 \pm 200$ nm and diameter $D_{core} = 62 \pm 3$ nm. Here, the uncertainties denote the standard deviations of the diameter and length distribution of the 20 NWs measured. Figure 1(b) shows a SEM image of this NW array.

3. Results and discussion

Figure 2(a) shows the measured reflectance R as a function of wavelength λ for the InAs substrate as well as the InAs NW array both initially and after each Al_2O_3 deposition step performed. In the reflectance of the substrate, we can identify the two well-known broad peaks at low wavelengths (at $\lambda \approx 475$ nm) that originate from the critical points in the band structure of InAs [24] at the L-point. In the range of Al_2O_3 coating thicknesses studied here, each deposition cycle of Al_2O_3 merely reduces the reflectance of the substrate (about 5%–7% for each of the four initial 10 nm cycles) in good agreement with analytical calculations [22] for multilayered systems (Fig. 2(b)).

The measured optical response of the bare/uncoated NW array (Fig. 2(a)) is very different from that of the substrate, as reported earlier in several studies [18, 25–27]. For all wavelengths investigated, the NW array shows much lower reflectance values than the substrate. This is in itself quite remarkable, considering that the NW array has only about 1% area coverage compared to a planar geometry, demonstrating the potential of dilute nanostructure arrays for tailoring

[1] We confirmed experimentally that the Al_2O_3 coating is uniform in the sense that it is equally thick on the sidewalls of the NWs, on top of the NWs, and on the substrate surface.

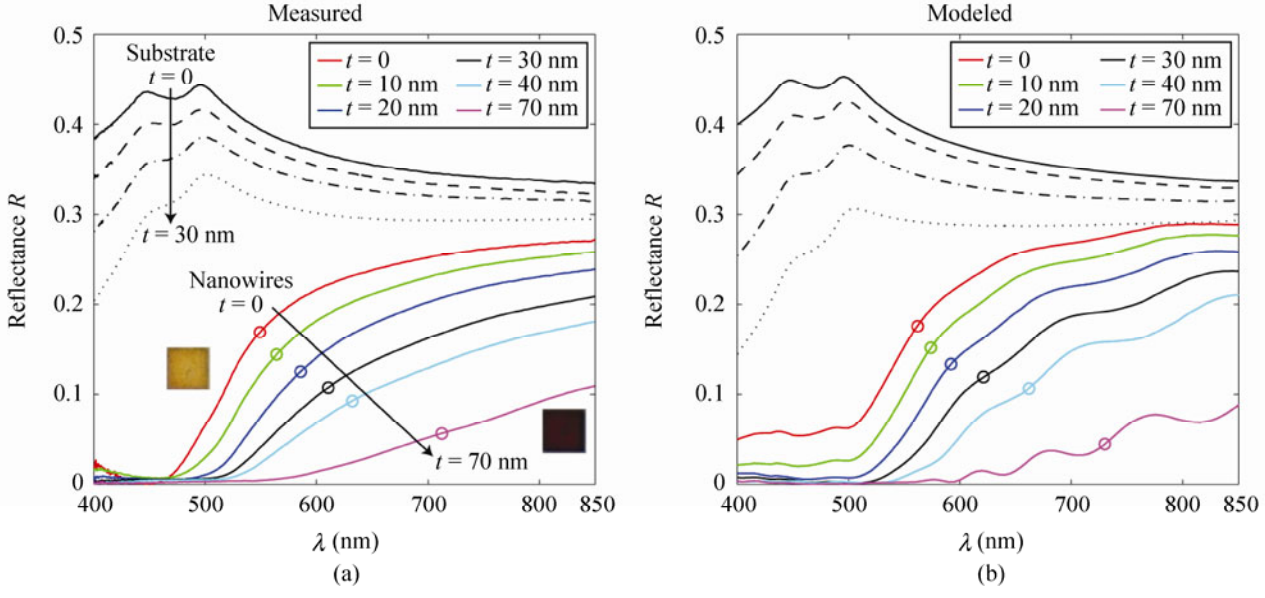

Figure 2 (a) Measured reflectance spectra of an InAs NW array of period p = 450 nm and NWs of diameter D_{core} = 62 nm and length L = 2040 nm for varying thickness t = 0, 10, 20, 30, 40, and 70 nm of the Al_2O_3 shell (see Fig. 1(a) for a schematic view). Here, also the reflectance of a bare InAs substrate is shown for varying Al_2O_3 coating layer thickness t = 0, 10, 20, and 30 nm. The two colorful inset squares are optical images of the NW array for t = 0 (left) and t = 70 nm (right). (b) Modeled reflectance spectra as a function of the Al_2O_3 coating thickness for the same geometries as in (a) obtained by numerically solving the Maxwell's equations. The open circles indicate $\lambda_{halfway}$ above (below) which the reflectance is high (low) (see text for details)

strongly the optical response in optoelectronic applications. The reflectance of the NW array is, similar as for the coated substrate, reduced with increasing thickness t of the Al_2O_3 coating layer. There is, however, at the same time also a large shift in the reflectance spectra towards longer wavelengths not found in the response of the substrate. As a qualitative measure for this spectral shift we define a characteristic halfway point $R_{halfway}$ for the reflectance with a corresponding wavelength $\lambda_{halfway}$ below (above) which the reflectance is lower (higher). Here, the halfway reflectance value is defined by $R_{halfway} = R(\lambda_{halfway})$ where $R_{halfway} = [R(\lambda = 850\text{ nm}) + R_{min}]/2$ and R_{min} is the minimum value of the reflectance for 500 nm < λ < 850 nm.[2] For the array of uncoated NWs, the $\lambda_{halfway}$ = 550 nm and $R_{halfway}$ = 17%. The $\lambda_{halfway}$ is then substantially shifted to longer wavelengths with increasing coating thickness. We observe a shift after the first and second coating cycle to $\lambda_{halfway}$ = 564 nm and $R_{halfway}$ = 14%; and $\lambda_{halfway}$ = 585 nm and $R_{halfway}$ = 12%, respectively. For t = 70 nm, when the thickness of the shell is comparable to the core diameter D_{core} = 62 nm, we observe that $\lambda_{halfway}$ has shifted to the red region of the visible wavelength range ($\lambda_{halfway}$ = 712 nm and $R_{halfway}$ = 5%). This strong shift of $\lambda_{halfway}$ causes a clear color change in the reflected light as compared to the bare/uncoated NW array; see insets in Fig. 2(a).

To accurately analyze the optical response, here specifically the reflectance and the absorptance, of the three-dimensional NW array system, we use numerical simulations based on the scattering matrix method [6, 18, 28] to solve Maxwell's equations. In short, we model the optical response of the NW array by employing tabulated values for the refractive index n of the Al_2O_3 [29] and the InAs [30]. The incident light is modeled as a plane wave incident from a direction specified by the polar angle θ_{inc} and the azimuth angle ϕ_{inc} (Fig. 1(a)). To model the experimental illumination (and collection) numerical aperture of NA = 0.5 (30° half angle), we averaged for 0° < θ_{inc} < 30° the response of both Transverse Electric (TE) and Transverse Magnetic (TM) polarized incident light to mimic the unpolarized light used in the experiments. In this

[2] This interval is chosen since there is a slight discrepancy between theory and experiments at low wavelengths of λ < 500 nm.

averaging, we considered contributions only from those reflected diffracted orders that propagated within the NA = 0.5 of the collection cone. To reduce the numerical burden, we fixed the azimuth angle ϕ_{inc} to 0° (since the results obtained for $\phi_{inc} = 0°$ differed only very slightly compared to the results obtained when using $\phi_{inc} = 45°$ instead (not shown), indicating a weak ϕ_{inc} dependence of the optical response).

Figure 2(b) shows the simulated reflectance as a function of wavelength λ for varying Al_2O_3 coating thickness t on top of a NW array with the same geometrical parameters as in the experiments (but excluding the Au particle which has been previously [18] shown to give only very minor contributions to the optical response of NW arrays of small core diameters). We obtain a very good agreement between the measured and modeled spectra for all coating thicknesses, especially for wavelengths larger than 500 nm. The simulated optical response of the NW array reproduces very well both the magnitude of the reduced reflectance and the red shift of the spectra with increasing coating thickness. However, a small oscillation pattern, not observed in measurements, can be seen in the modeled spectra. We have verified (not shown) that these oscillations in the modeling stem from interference between light reflected at the top-interface (top of the coated NWs) and light reflected at the NW/substrate bottom interface. As one would intuitively expect, the magnitude of the top interface reflectance, and therefore its ability to modulate the total reflectance, becomes larger with increasing number of oxide deposition cycles (or in other words, increasing area coverage). This explains why the oscillations in the modeled reflectance spectra in Fig. 2(b) are the strongest for the thickest Al_2O_3 layer. Interference is however inherently very sensitive to the phase of the reflected light, and for example differences in optical path length can randomize the phase and destroy interference effects. Therefore, the rather large experimental NW length distribution with standard deviation of 200 nm (corresponding to approximately $\pm \lambda/4$) is expected to wash out such oscillations from the experiments, explaining the lack of oscillations in the measured reflectance spectra in Fig. 2(a). Reduced reflectance is one of the key factors for achieving highly efficient optical components for photodetection and photovoltaics, and as shown above both experimentally and theoretically, we can achieve this reduction in NW array based devices by coating the NWs with a dielectric. It is however even more important that the light coupled into the device is absorbed in the active region. For many applications with NWs, the active region is located in the NWs [4, 5, 7, 31] and absorption in the substrate does not contribute to the performance of the device. Thus, we wish to study how the dielectric coating affects the absorptance of the NWs. The very good agreement found in Fig. 2 between the measured and modeled reflectance convincingly shows that the theoretical framework accurately describes the optical response of the NW arrays, including the absorption of light.

By employing energy balance, the absorptance A of the NWs can be obtained by $A(\lambda) = 1 - R_{tot}(\lambda) - T_{tot}(\lambda)$ where $R_{tot}(\lambda)$ is the (total) reflectance of the NW array and $T_{tot}(\lambda)$ is the transmittance into the InAs substrate. Hence, the theoretical modeling allows us to study how much light is absorbed in just the NWs, which is not accessible from experimental measurements due to the thick, absorbing substrate.

Figure 3 shows how the absorptance (of the NWs) increases strongly as the thickness of the non-absorbing Al_2O_3 shell is increased, without changing the size or shape of the absorbing InAs core of the NWs. For a central wavelength of 600 nm the absorptance is enhanced by more than 150% for $t = 70$ nm, the thickest layer deposited experimentally. By comparing Figs. 2 and 3, we conclude that the shape and shift of the reflectance spectrum are directly complementary to those of the absorptance spectrum, thus demonstrating that the observed reflectance originates mainly from light that is reflected at the NW/substrate bottom interface and absorbed during the round-trip through the NW array.

The trend of increasing absorptance with increasing t presented in Fig. 3, where the Al_2O_3 coating thickness $t \leqslant 70$ nm, can easily lead one to think that the absorptance increases monotonically with increasing t until the space between the NWs is completely filled with Al_2O_3. We will in the following show that this is *not* the case. Instead, there is an *optimum* shell thickness to aim for when improving the absorptance of the NWs.

To first gain an intuitive picture of why the

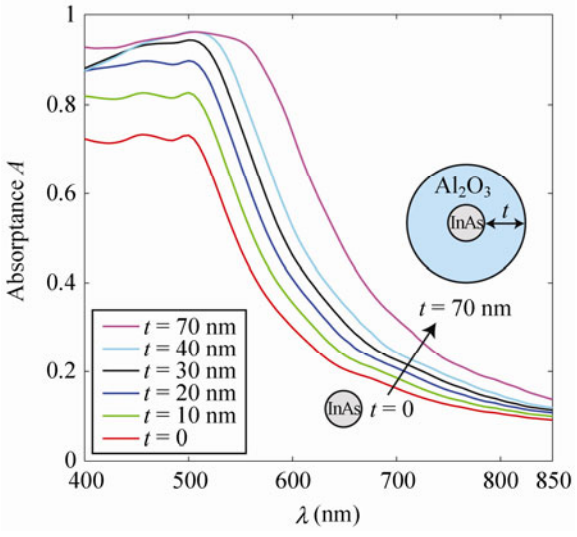

Figure 3 Modeled absorptance A of the InAs NW array whose reflectance is shown in Fig. 2 (period p = 450 nm, InAs NW core diameter D_{core} = 62 nm, and NW length L = 2040 nm) for increasing thickness t = 0, 10, 20, 30, 40, and 70 nm of the Al_2O_3 shell (see Fig. 1(a) for a schematic view). Here, the absorptance of light incident from a cone of 30° half-angle is averaged in the modeling to correspond to the objective lens of NA = 0.5 used in the measurements in Fig. 2

absorptance increases when increasing the thickness t of the non-absorbing Al_2O_3 shell, we start with an electrostatic approximation [32]. We limit the discussion to how the electric field of the incident light penetrates into the core of a single InAs NW (considered here as an infinitely long cylinder) with a core diameter D_{core} of 62 nm for incident light of wavelength λ = 850 nm. We set the (total) electric field $\boldsymbol{E}$ far away from the single NW equal to the incident electric field $\boldsymbol{E}_{inc}$. We consider the cases of t = 0 (no shell; Fig. 4(a)) and t = 150 nm (a 150 nm thick Al_2O_3 shell; Fig. 4(b)). We note that for $\boldsymbol{E}_{inc} = (E_0,0,0)$, when the axis of the NW is along the z direction, the electric field in the NW core, $\boldsymbol{E}_{core}$, is constant and x-polarized. In the absence of a shell (Fig. 4(a)), the incident electric field intensity is screened from the interior of the NW by the factor of $|\boldsymbol{E}_{core}/\boldsymbol{E}_{inc}|^2 = |2\varepsilon_{ext}/(\varepsilon_{ext}+\varepsilon_{core})|^2 \approx 0.018$ where ε_{ext} = 1 is the (relative) dielectric function of the vacuum exterior to the NW and $\varepsilon_{core} \approx 13.6 + 3.16i$ is the dielectric function (for λ = 850 nm) of the InAs core. This strong screening of the (incident) electric field from the NW core occurs due to the strong contrast in the values of the dielectric functions of the exterior and the core: The incident electric field causes a surface charge

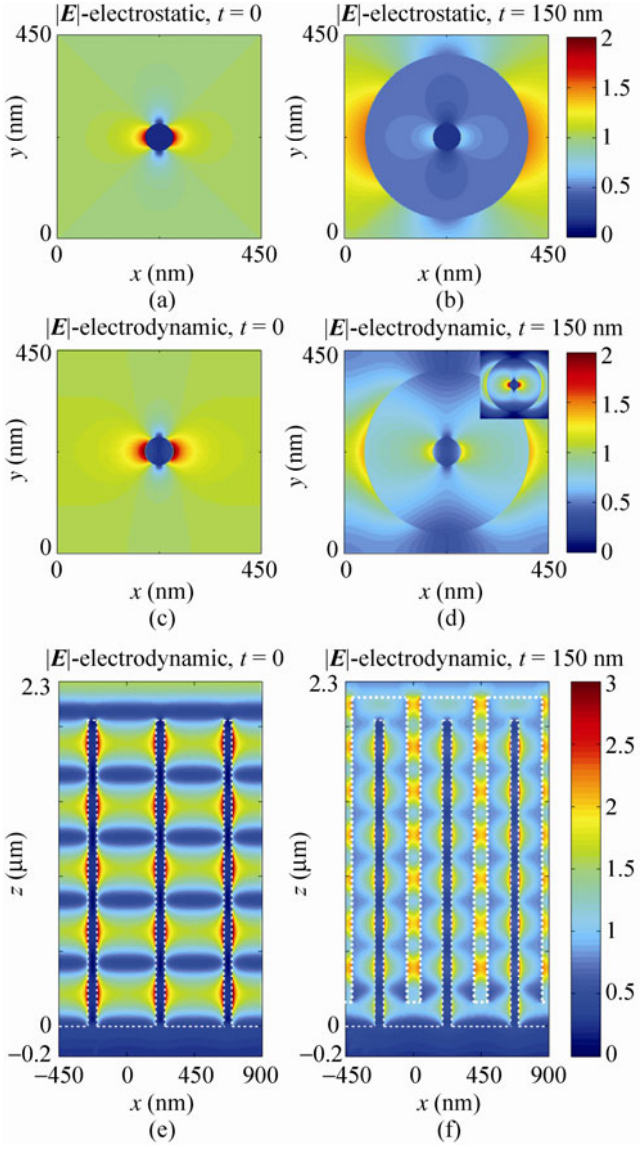

Figure 4 (a) Electric field $|\boldsymbol{E}|$ calculated in the electrostatic approximation for an InAs NW with a core diameter D_{core} = 62 nm (and no shell). The incident light is x-polarized with $|\boldsymbol{E}_{inc}|$ = 1 V/m, the NW axis is in the z direction, and the dielectric function of InAs for λ = 850 nm was used. Here, the electric field in the core has the value of $|\boldsymbol{E}_{core}|$ = 0.134 V/m. (b) Same as (a) but now also including a 150 nm thick Al_2O_3 shell. Here, $|\boldsymbol{E}_{core}|$ = 0.177 V/m, and thus the electric field strength in the NW core is noticeably higher than without the shell. (c)–(d): Same as for (a) and (b) but from full electrodynamic modeling at $z = L/4$ for a NW array with p = 450 nm, D_{core} = 62 nm, and L = 2040 nm. The inset in (d) shows the semi-analytically calculated electric field of the fundamental HE11 waveguide mode of a single core–shell NW. (e) and (f): Same as (c) and (d) but for a cross-section in the x–z plane through the centers of three NWs. The dashed lines indicate the InAs NW core and the Al_2O_3 shell

layer at the boundary of the NW core, which partially screens the electric field from the interior of the NW. We expect intuitively that a shell, of a material having a dielectric function with a value between that of those of the core and the exterior, might weaken this strong screening. Indeed, when we consider the case of the 150 nm thick Al_2O_3 shell of $\varepsilon_{shell} = 3.09$ (Fig. 4(b)), the intensity in the core increases to $|\boldsymbol{E}_{core}/\boldsymbol{E}_{inc}|^2 \approx 0.031$. Thus, we expect a noticeably higher absorptance in the presence of the shell since the absorption is proportional[18] to $|\boldsymbol{E}_{core}|^2$, which is here enhanced by a factor of 1.7 when adding the 150 nm thick shell. This enhancement factor increases monotonously with increasing shell thickness toward the limiting value of 1.8 (Fig. S-1 in the Electronic Supplementary Material (ESM)). Thus, this intuitive electrostatic analysis explains why the absorptance in Fig. 3 increases with t. Furthermore, we are lead also here to expect that the absorptance of the NW array increases monotonously with increasing shell thickness, which would in turn imply that simply filling the space between the NWs completely with Al_2O_3 would give the maximum enhancement of the absorptance.

However, when we study (with full electrodynamic modeling [28]) the absorptance as a function of shell thickness t, a radically different picture emerges (Fig. 5). Here, we turn to consider the case of normally incident light ($\theta_{inc} = 0$) which maximizes the projected area of a nanowire array to the incident light. As expected from the electrostatic approximation, and already shown in Fig. 3 for $t \leqslant 70$ nm, the absorptance increases initially with t when starting from uncoated NWs. But in strong contrast to the expectation above of a monotonous increase, the absorptance instead peaks for an intermediate value of t (the small oscillation overlaid on the curve are due to interference of light inside the NW layer, see Figs. S-6 and S-7 in ESM). We notice that the peak shifts toward larger t with increasing λ (Figs. 5(b)–5(d)). This peak is broad, implying that for a broad range in t, the absorptance is much higher than even at $t = 287$ nm where the space between the NWs is completely filled with Al_2O_3. We note that the absorptance at $t = 287$ nm is approximately a factor of 2 higher than for the case of bare/uncoated NWs at $t = 0$, in good agreement with

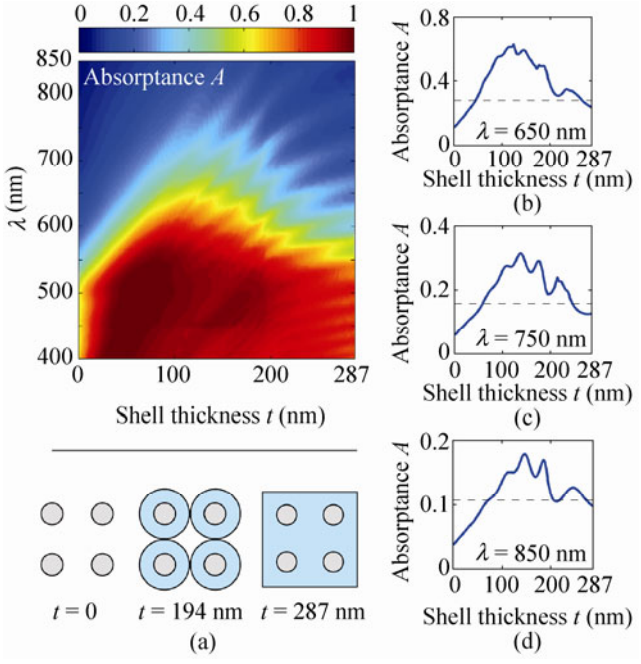

Figure 5 (a) Absorptance A of an InAs NW array of period p = 450 nm and NWs of core diameter D_{core} = 62 nm and length L = 2040 nm as a function of Al_2O_3 shell thickness t and wavelength λ (see Fig. 1(a) for a schematic view). Here, we consider normally incident light ($\theta_{inc} = 0$). As depicted schematically at the bottom, the shells of neighboring NWs start to touch each other at t = 194 nm and the space between the NWs is completely filled with Al_2O_3 at t = 287 nm, the largest thickness considered here. (b), (c), and (d): Line-cuts from (a) at λ = 650, 750, and 850 nm (solid blue line). The dashed line shows the absorptance of the corresponding NW array when Al_2O_3 fills all the space between and above the NWs; and the light is incident directly from the Al_2O_3, which is optically equivalent to a perfect anti-reflection coating at the air/Al_2O_3 interface at the top (Fig. S-2 in the ESM)

the factor of 1.8 derived above with the electrostatic approximation. Thus, to understand the origin of this peak of the absorptance, we must turn to electrodynamic considerations.

One case, for which electrostatics fails to give an accurate description of the interaction of light with an optical system, is when constructive interference plays role. One particular possibility for such interference inside a NW is for light that circulates in the (circular) cross-section of the NW. If we by $D_{tot} = D_{core} + 2t$ denote the total diameter of a core–shell NW, then an approximate condition for such constructive interference is $\pi(D_{tot}/2)n_{NW}2\pi/\lambda = 2\pi m$ with m an integer and n_{NW} a refractive index that describes the NW. This condition corresponds to light that circulates at r =

$D_{tot}/4$, that is, halfway between the center and the boundary of the NW. With $m = 1$, the constructive interference in the cross-section corresponds here to the fundamental waveguide mode (HE11) of the core–shell NW (see inset in Fig. 4(d)). We obtain in this case $D_{tot} = 2\lambda/(n_{NW}\pi) \approx 240$ nm for $\lambda = 650$ nm and $n_{NW} \approx 1.75$ for which we assumed that the main contribution of the optical response of the NW comes from a thick Al_2O_3 shell of refractive index $n \approx 1.75$. For the case of $D_{core} = 62$ nm in Fig. 5, $D_{tot} = 240$ nm corresponds to a shell thickness $t \approx 90$ nm, in good agreement with the region of t where we observe the absorptance peak in Fig. 5(b) (we do not expect exact quantitative agreement since we use such a rough approximation for the resonance condition). The approximated resonant diameter shifts linearly to $D_{tot} = 310$ nm when the wavelength is increased to $\lambda = 850$ nm, and the resulting $t \approx 125$ nm agrees well with the location of the peak for $\lambda = 850$ nm in Fig. 5(d).

To quantitatively investigate why the electrostatic approximation fails to reproduce the peak of A as a function of t in Fig. 5, we show in Fig. 4(c) for $t = 0$ and in Fig. 4(d) for $t = 150$ nm the electric fields calculated with full electrodynamics (Finite Difference Time Domain (FDTD), Lumerical package) for $\lambda = 850$ nm. We find for the uncoated case of $t = 0$ nm (Fig. 4(c)) an electric field distribution that is very similar to the distribution obtained with the electrostatic approximation in Fig. 4(a). However, for $t = 150$ nm (Fig. 4(d)), there is a strongly non-uniform electric field distribution inside both the shell and the core of the NW, which differs considerably from the field distribution obtained with the electrostatic approximation (Fig. 4(b)). This difference explains why electrostatics fails in describing the optical response (the peak of A) of the system for larger values of t. To corroborate the qualitative claim above that the peak in A for $t \approx 150$ nm is caused by resonant excitation of the HE_{11} waveguide mode, we show in the inset of Fig. 4(d) the electric field distribution of the HE_{11} waveguide mode [33] of a single core–shell NW. The field distribution of this mode matches very closely the modeled distribution in the NW array (Fig. 4(d)), corroborating the above qualitative claim. We have verified (not shown) that the slight differences (especially noticeable in the exterior outside the shell) in the electric field distribution of the NW array compared to that of the HE_{11} mode of the single NW are mainly caused by contributions from the HE_{11} modes of neighboring NWs in the array.

To analyze in more detail the electric field distribution in the whole NW (instead of the selected x–y cross-section in Figs. 4(c) and 4(d)), we show the electric field ($|\boldsymbol{E}|$) in a side-view cross-section through the centers of three NWs in Fig. 4(e) for bare/uncoated NWs and in Fig. 4(f) for NWs with a 150 nm thick Al_2O_3 shell. For both cases, it is apparent that the field in the NW core is highly non-uniform along the z direction, and the field strength as well as the number of nodes changes when adding the Al_2O_3 shell. To quantitatively study this node structure, we have first calculated the average electric field $\langle|\boldsymbol{E}|^2\rangle_{core}$ in the NW core as a function of z along the NW axis (Fig. S-3 in the ESM). We found strong but nearly uniform oscillations with a visibility of approximately 0.2 for the bare/uncoated NWs and 0.35 for the NWs with a 150 nm thick Al_2O_3 shell. Next, we found that the mean value of the electric field inside the bare/uncoated NWs was $\langle|\boldsymbol{E}|^2\rangle_{NW} = 0.053$ (calculated as the average of $\langle|\boldsymbol{E}|^2\rangle_{core}$ over z). For the NWs with a 150 nm thick Al_2O_3 shell, $\langle|\boldsymbol{E}|^2\rangle_{NW} = 0.25$. Thus, the 150 nm thick Al_2O_3 shell leads to a 4.8 times larger average value of $|\boldsymbol{E}|^2$ inside the NWs. This explains the strong enhancement in absorptance by the same factor of 4.8 in Fig. 5 when we add a 150 nm thick shell to an uncoated NW (since the local absorption at any position inside the NW core is proportional to $|\boldsymbol{E}(\boldsymbol{r})|^2$ so that the absorptance is proportional to $\langle|\boldsymbol{E}|^2\rangle_{NW}$).

To summarize, we have found that coating a bare semiconductor NW with a non-absorbing dielectric shell increases the absorptance, as expected from electrostatic considerations of the screening of the incident electric field from the interior of a high refractive index cylinder (that is, the InAs NW core). By completely filling the space between the NWs with Al_2O_3, the absorptance can be increased by a factor of two. However, we found that stopping at an intermediate shell thickness can boost the absorptance by an additional factor of two from this value. Thus, by using a dielectric shell, the absorptance can be enhanced by a factor of four compared to the case of completely uncoated NWs, see Table 1.

Table 1 Absorptance of InAs NWs with diameter D_{core} = 62 nm and length L = 2040 nm placed in a square array of period p = 450 nm on top of an InAs substrate (data from Fig. 5)

Wavelength	Absorptance of uncoated NW array	Absorptance of completely Al_2O_3 covered NW array	Peak absorptance and corresponding Al_2O_3 shell thickness
λ = 650 nm	A = 11%	A = 28%	A = 63% @ t =124 nm
λ = 750 nm	A = 6%	A = 16%	A = 32% @ t =138 nm
λ = 850 nm	A = 4%	A = 11%	A = 18% @ t = 147 nm

Since, as demonstrated above (Figs. 5(b)–5(d)), the resonance condition giving enhanced absorption for a given λ is broad in shell thickness t, we expect similarly enhanced absorption in a broadband wavelength range for a suitable choice of t. To demonstrate this, we show in Fig. 6 for 400 nm < λ < 850 nm the absorptance after an optimized choice for the shell thickness t. This optimized shell thickness of t = 115 nm was determined by maximizing the average of $A(\lambda)$ over 400 nm < λ < 850 nm. We find that the absorptance is increased considerably compared to the case of no shell (t = 0) and the case when the Al_2O_3 covers completely the NWs, that is, when t = 287 nm. Specifically, we find with this optimized shell thickness an average increase of 140% in $A(\lambda)$ compared to the case of no shell, an increase by more than 300% for λ > 600 nm, and a peak increase by 450% at λ = 700 nm.

We have so far investigated the optical response of the NW array by changing the thickness of the surrounding dielectric shell. One might argue that changing the NW core diameter, the NW length or the array period could have similar effects. We have studied these situations in detail (see the ESM). First, there is a strong increase in the absorptance when increasing the NW core diameter, as reported previously for uncoated NWs [18]. For an array where the NW core diameter is 62 nm, the absorptance is approximately 4% at λ = 850 nm (Table 1), which is improved to 26% when increasing the NW core diameter to 102 nm (Fig. S-4 in the ESM). However, also for this increased core diameter, the addition of an appropriate thickness of Al_2O_3 coating increases the absorptance considerably, in this case to 70% (Table S-1 in the ESM). Second, to understand the influence of the NW length on the absorptance, we adopt a simplified model assuming the excitation of a single absorbing optical mode in the NW array. We deduce that when the absorptance is much smaller than unity, there is a linear dependence of the absorptance on the NW length (as seen by retaining only the linear term in the expansion of the exponential absorption function). Thus, if the absorptance is doubled by adding a dielectric shell (with t ~ 100–200 nm; see Fig. 5), twice as long NW length L would be required to reach the same increase if L was varied instead. However, even when the NW length is increased, the absorptance can still be enhanced with a shell. Third, we have found that an increase of the period by 100 nm, corresponding to a decrease of the area coverage by 30%, causes only slight changes in the absorptance (Fig. S-6 in the ESM), in good agreement with previous modeling of the absorption efficiency of uncoated InP NW arrays [8], showing that the period is for the absorptance the least significant of these three geometrical parameters.

From a technological point of view, increasing the NW length considerably could become an issue since the NWs can start to stick together mechanically [34], and this could cause unpredictable/non-reproducible behavior in later steps of device processing. Furthermore, in photovoltaic and photodetection applications with axial pn-junctions, electron-hole recombination in the depletion region might become a performance limiting issue if the NW length (and therefore the length of the depletion region) is excessively increased. Increasing the NW core diameter can be a very suitable option, but beyond a material-combination dependent critical diameter, (performance limiting) dislocations start to show up when materials of dissimilar crystal lattice constants are combined [13, 35]. This can strongly limit the possible material combinations for more advanced heterostructures and make large diameter NWs tricky to grow on cheap substrates [36–38]. However, as discussed above, even if the NW diameter or length can be increased, the dielectric coating still offers a drastic boost to the absorptance.

Lastly, structural defects at the interface between the dielectric shell and the NW core could cause non-radiative recombination and lead to suboptimal performance in opto-electronic devices. Such problems could be alleviated by first surface passivating the NW

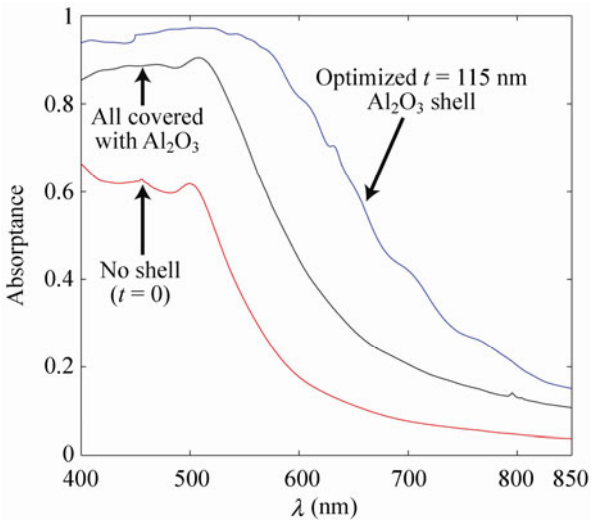

Figure 6 Modeled absorptance A of an InAs NW array of period p = 450 nm, InAs NW core diameter D_{core} = 62 nm, and NW length L = 2040 nm and three different cases for the Al_2O_3 shell: (i) t = 0, that is, no shell, (ii) t = 115 nm, which maximizes the average value of $A(\lambda)$ over 400 nm < λ < 850 nm, and (iii) the Al_2O_3 fills all the space between and above the NWs; and the light is incident directly from the Al_2O_3, which is optically equivalent to t = 287 nm and a perfect anti-reflection coating at the air/Al_2O_3 interface at the top (Fig. S-3 in the ESM). Here, we consider normally incident light (that is, θ_{inc} = 0)

core with a high-band gap encapsulation material [39] to move the structural defects away from the active region.

4. Conclusions

In conclusion, we have shown how a non-absorbing (dielectric) Al_2O_3 shell can drastically increase the absorption of light in a vertical InAs semiconductor NW array. In all systems investigated, we observed that the dielectric shell greatly improves the coupling of light into the absorbing NW core. More importantly, we found a broad resonance condition in shell thickness (Figs. 5(b)–5(d)) with a peak absorption enhancement by a factor of four compared to uncoated NWs. By aiming for this resonance condition, it is possible to achieve strong absorption enhancement for a broad wavelength range without increasing the amount or shape of the absorbing semiconductor material in the NW core (Fig. 6). This resonance condition originates from constructive interference in the NW cross-section, and to describe this, we derived a simple approximate formula that depends only on the refractive index and geometrical dimensions of the cross-section. Thus, our reported absorption enhancement is not limited to the particular NW and coating layer materials nor to the wavelength range chosen for this study. Instead, with an appropriate choice for the shell thickness, the enhancement can be tuned to different wavelength ranges and employed in other material systems, also outside the realm of Ⅲ–Ⅴ semiconductors.

Methods

Core–shell InAs–Al_2O_3 nanowire array fabrication. InAs NW arrays of 50 μm × 50 μm in area and square lattice were grown in a CBE unit. The Au dots of each array were defined by EBL. Tertiarybutylarsine (TBA) was thermally cracked into As at an As ambient of 1.5 mbar, and at the growth temperature of 425 ℃, 0.15 mbar of Trimethylindium (TMIn) was introduced to initiate the growth of the NWs. At the end of the growth, the TMIn flow to the chamber was shut and the samples were allowed to cool to nearly room temperature in As ambient background before removing the samples from the CBE unit. To form the dielectric shell, Al_2O_3 was deposited by ALD (Cambridge Nanotech Savannah system) at 250 ℃.

Reflectance measurements. Reflectance measurements were performed for 400 nm < λ < 850 nm with a Filmetrics F40 optical probe attached to a Zeiss Axio Imager M1m optical microscope. The incident light was sent in normal to the array using a 20x objective (NA = 0.5). The reflected light was collected with the same objective from a square spot of an area of 20 μm × 20 μm.

Electrodynamic modeling. Numerical simulations based on the scattering matrix method [6, 18, 28] to solve Maxwell's equations were used to obtain the optical spectra (reflectance, transmittance, and absorptance) of the core–shell NW array system. Tabulated values for the refractive index n of the Al_2O_3 [29] and the InAs [30] were used, and for the air, n = 1 was assumed. The incident light was modeled as a plane wave of a given wavelength incident from a direction specified by the polar angle θ_{inc} and the

azimuth angle ϕ_{inc}. To model the NA = 0.5 of the objective used in the measurements, we averaged over incidence angles and polarizations as described in detail in the main text. Electric field distributions were calculated with the FDTD method (Lumerical package).

Acknowledgments

We acknowledge George Rydnemalm, Mariusz Graczyk and Sören Jeppesen for assistance in sample processing and Professors Lars Samuelson, Heiner Linke, and Mats–Erik Pistol for stimulating discussions and support. This work was financially supported by the Swedish Research Council (VR), the Swedish Foundation for Strategic Research (SSF), the Nanometer Structure Consortium at Lund University (nmC@LU), European Union (EU) program Architectures, Materials, and One-dimensional Nanowires for Photovoltaics-Research and Applications (AMON-RA) (No. 214814), Nordic Innovation program NANORDSUN, Knut and Alice Wallenberg Foundation, E.ON AG as part of the E.ON International Research Initiative, the National Basic Research Program of the Ministry of Science and Technology of China (Nos. 2012CB932703 and 2012CB932700), and a Fellowship for Young International Scientists of Chinese Academy of Sciences (U. H.).

Electronic Supplementary Material: Supplementary material on limiting values of electric field penetration into NW core in the electrostatic approximation, effects of antireflection coating on absorptance of nanowire arrays, average $|\boldsymbol{E}|^2$ in the x–y cross section of the nanowire core, diameter dependence of the absorptance in the nanowire arrays, period dependence of the absorptance in the nanowire arrays, and absorptance peaks and dips due to interference in nanowire layer is available in the online version of this article at http://dx.doi.org/10.1007/s12274-012-0270-x.

References

[1] Fan, H. J.; Werner, P.; Zacharias, M. Semiconductor nanowires: From self-organization to patterned growth. *Small* **2006**, *2*, 700–717.

[2] Martensson, T.; Carlberg, P.; Borgström, M.; Montelius, L.; Seifert, W.; Samuelson, L. Nanowire arrays defined by nanoimprint lithography. *Nano Lett.* **2004**, *4*, 699–702.

[3] Goto, H.; Nosaki, K.; Tomioka, K.; Hara, S.; Hiruma, K.; Motohisa, J.; Fukui, T. Growth of core–shell InP nanowires for photovoltaic application by selective-area metal organic vapor phase epitaxy. *Appl. Phys. Express* **2009**, *2*, 035004.

[4] Fukui, T.; Yoshimura, M.; Nakai, E.; Tomioka, K. Position-controlled Ⅲ–Ⅴ compound semiconductor nanowire solar cells by selective-area metal–organic vapor phase epitaxy. *AMBIO* **2012**, *41*, 119–124.

[5] Czaban, J. A.; Thompson, D. A.; LaPierre, R. R. GaAs core−shell nanowires for photovoltaic applications. *Nano Lett.* **2009**, *9*, 148–154.

[6] Anttu, N.; Xu, H. Q. Coupling of light into nanowire arrays and subsequent absorption. *J. Nanosci. Nanotechnol.* **2010**, *10*, 7183–7187.

[7] Borgström, M. T.; Wallentin, J.; Heurlin, M.; Fält, S.; Wickert, P.; Leene, J.; Magnusson, M. H.; Deppert, K.; Samuelson, L. Nanowires with promise for photovoltaics. *IEEE J. Sel. Top. Quant.* **2011**, *17*, 1050–1061.

[8] Kupec, J.; Stoop, R. L.; Witzigmann, B. Light absorption and emission in nanowire array solar cells. *Opt. Express* **2010**, *18*, 27589–27605.

[9] Diedenhofen, S. L.; Janssen, O. T. A.; Grzela, G.; Bakkers, E. P. A. M.; Rivas, J. G. Strong geometrical dependence of the absorption of light in arrays of semiconductor nanowires. *ACS Nano* **2011**, *5*, 2316–2323.

[10] Logeeswaran, V. J.; Oh, J.; Nayak, A. P.; Katzenmeyer, A. M.; Gilchrist, K. H.; Grego, S.; Kobayashi, N. P.; Wang, S. Y.; Talin, A. A.; Dhar, N. K.; Islam, M. S. A perspective on nanowire photodetectors: Current status, future challenges, and opportunities. *IEEE J. Sel. Top. Quant.* **2011**, *17*, 1002–1032.

[11] Scofield, A. C.; Kim, S. H.; Shapiro, J. N.; Lin, A.; Liang, B. L.; Scherer, A.; Huffaker, D. L. Bottom-up photonic crystal lasers. *Nano Lett.* **2011**, *11*, 5387–5390.

[12] Svensson, C. P. T.; Martensson, T.; Tragardh, J.; Larsson, C.; Rask, M.; Hessman, D.; Samuelson, L.; Ohlsson, J. Monolithic GaAs/InGaP nanowire light emitting diodes on silicon. *Nanotechnology* **2008**, *19*, 305201.

[13] Kästner, G.; Gösele, U. Stress and dislocations at cross-sectional heterojunctions in a cylindrical nanowire. *Philos. Mag.* **2004**, *84*, 3803–3824.

[14] Dick, K. A.; Kodambaka, S.; Reuter, M. C.; Deppert, K.; Samuelson, L.; Seifert, W.; Wallenberg, L. R.; Ross, F. M. The morphology of axial and branched nanowire heterostructures. *Nano Lett.* **2007**, *7*, 1817–1822.

[15] Björk, M. T.; Ohlsson, B. J.; Sass, T.; Persson, A. I.; Thelander, C.; Magnusson, M. H.; Deppert, K.; Wallenberg, L. R.; Samuelson, L. One-dimensional steeplechase for electrons realized. *Nano Lett.* **2002**, *2*, 87–89.

[16] Lauhon, L. J.; Gudiksen, M. S.; Wang, C. L.; Lieber, C. M. Epitaxial core–shell and core–multishell nanowire heterostructures. *Nature* **2002**, *420*, 57–61.

[17] Green, M. A. Third generation photovoltaics: Ultra-high conversion efficiency at low cost. *Prog. Photovoltaics* **2001**, *9*, 123–135.

[18] Wu, P. M.; Anttu, N.; Xu, H. Q.; Samuelson, L.; Pistol, M. E. Colorful InAs nanowire arrays: From strong to weak absorption with geometrical tuning. *Nano Lett.* **2012**, *12*, 1990–1995.

[19] Marichy, C.; Bechelany, M.; Pinna, N. Atomic layer deposition of nanostructured materials for energy and environmental applications. *Adv. Mater.* **2012**, *24*, 1017–1032.

[20] Persson, H.; Beech, J. P.; Samuelson, L.; Oredsson, S.; Prinz, C. N.; Tegenfeldt, J. O. Vertical oxide nanotubes connected by subsurface microchannels. *Nano Res.* **2012**, *5*, 190–198.

[21] Schmidt, J.; Veith, B.; Brendel, R. Effective surface passivation of crystalline silicon using ultrathin Al_2O_3 films and Al_2O_3/SiN*x* stacks. *Phys. Status Solidi-R* **2009**, *3*, 287–289.

[22] Macleod, H. A. *Thin-Film Optical Filters;* CRC Press: New York, 2010.

[23] Min, B. D.; Lee, J. S.; Cho, K. G.; Hwang, J. W.; Kim, H.; Sung, M. Y.; Kim, S.; Park, J.; Seo, H. W.; Bae, S. Y.; Lee, M. S.; Park, S. O.; Moon, J. T. Semiconductor nanowires surrounded by cylindrical Al_2O_3 shells. *J. Electron. Mater.* **2003**, *32*, 1344–1348.

[24] *The Landolt Börnstein Database* [Online]. Springer Materials. http://www.springermaterials.com.

[25] Seo, K.; Wober, M.; Steinvurzel, P.; Schonbrun, E.; Dan, Y. P.; Ellenbogen, T.; Crozier, K. B. Multicolored vertical silicon nanowires. *Nano Lett.* **2011**, *11*, 1851–1856.

[26] Hu, L.; Chen, G. Analysis of optical absorption in silicon nanowire arrays for photovoltaic applications. *Nano Lett.* **2007**, *7*, 3249–3252.

[27] Muskens, O. L.; Rivas, J. G.; Algra, R. E.; Bakkers, E. P. A. M.; Lagendijk, A. Design of light scattering in nanowire materials for photovoltaic applications. *Nano Lett.* **2008**, *8*, 2638–2642.

[28] Anttu, N.; Xu, H. Q. Scattering matrix method for optical excitation of surface plasmons in metal films with periodic arrays of subwavelength holes. *Phys. Rev. B* **2011**, *83*, 165431.

[29] Palik, E. D.; Holm, R. T. Indium rsenide (InAs). In *Handbook of Optical Constants of Solids*, Palik, E. D., Ed.; Academic Press: Burlington, 1997; pp 479–489.

[30] Gervais, F. Aluminum Oxide (Al_2O_3). In *Handbook of Optical Constants of Solids*. Palik, E. D., Ed.; Academic Press: Burlington, 1997; pp 761–775.

[31] Tian, B. Z.; Zheng, X. L.; Kempa, T. J.; Fang, Y.; Yu, N. F.; Yu, G. H.; Huang, J. L.; Lieber, C. M. Coaxial silicon nanowires as solar cells and nanoelectronic power sources. *Nature* **2007**, *449*, 885–889.

[32] Nicorovici, N. A.; McPhedran, R. C.; Milton, G. W. Transport properties of a three-phase composite material: The square array of coated cylinders. *Proc. R. Soc. Lond. A* **1993**, *442*, 599–620.

[33] Bures, J. *Guided Optics: Optical Fibers and All-Fiber Components;* Wiley-VCH: Weinheim, 2009.

[34] Wu, P. M.; Samuelson, L.; Linke, H. Toward 3D integration of 1D conductors: Junctions of InAs nanowires. *J. Nanomater.* **2011**, 268149.

[35] Kavanagh, K. L. Misfit dislocations in nanowire heterostructures. *Semicond. Sci. Technol.* **2010**, *25*, 024006.

[36] Ghalamestani, S. G.; Johansson, S.; Borg, B. M.; Lind, E.; Dick, K. A.; Wernersson, L. E. Uniform and position-controlled InAs nanowires on 2″ Si substrates for transistor applications. *Nanotechnology* **2012**, *23*, 015302.

[37] Mårtensson, T.; Svensson, C. P. T.; Wacaser, B. A.; Larsson, M. W.; Seifert, W.; Deppert, K.; Gustafsson, A.; Wallenberg, L. R.; Samuelson, L. Epitaxial Ⅲ–Ⅴ nanowires on silicon. *Nano Lett.* **2004**, *4*, 1987–1990.

[38] Bakkers, E. P. A. M.; Borgström, M. T.; Verheijen, M. A. Epitaxial growth of Ⅲ–Ⅴ nanowires on group IV substrates. *MRS Bull.* **2007**, *32*, 117–122.

[39] Parkinson, P.; Joyce, H. J.; Gao, Q.; Tan, H. H.; Zhang, X.; Zou, J.; Jagadish, C.; Herz, L. M.; Johnston, M. B. Carrier lifetime and mobility enhancement in nearly defect-free core−shell nanowires measured using time-resolved terahertz spectroscopy. *Nano Lett.* **2009**, *9*, 3349–3353.